Supporting Information

Donor-Modified Asymmetric N/B/O Multi-Resonance TADF Emitters for High-Performance Deep-Blue OLEDs with BT.2020 Color Gamut

Jing Jin,[a,†] Zhaolong He,[a,†] Di Liu,*[a] Yongqiang Mei,[c] Jiahui Wang,[c] Huihui Wan,[d] Jiuyan Li,*[b,c]

[a] Frontier Science Center for Smart Materials, College of Chemistry, Dalian University of Technology, 2 Linggong Road, Dalian, 116024, China.

Email: liudi@dlut.edu.cn

[b] Shandong Laboratory of Yantai Advanced Materials and Green Manufacturing, Yantai Economic and Technological Development Zone, 300 Changjiang Road, Yantai, China.

Email: greenjiuyanli@amgm.ac.cn

[c] Frontier Science Center for Smart Materials, College of Chemical Engineering, Dalian University of Technology, 2 Linggong Road, Dalian, 116024, China.

[d] Instrumental Analysis Center, Dalian University of Technology, Dalian, 116024, China

† These authors contributed equally to this work.

Contents

1. Background Information

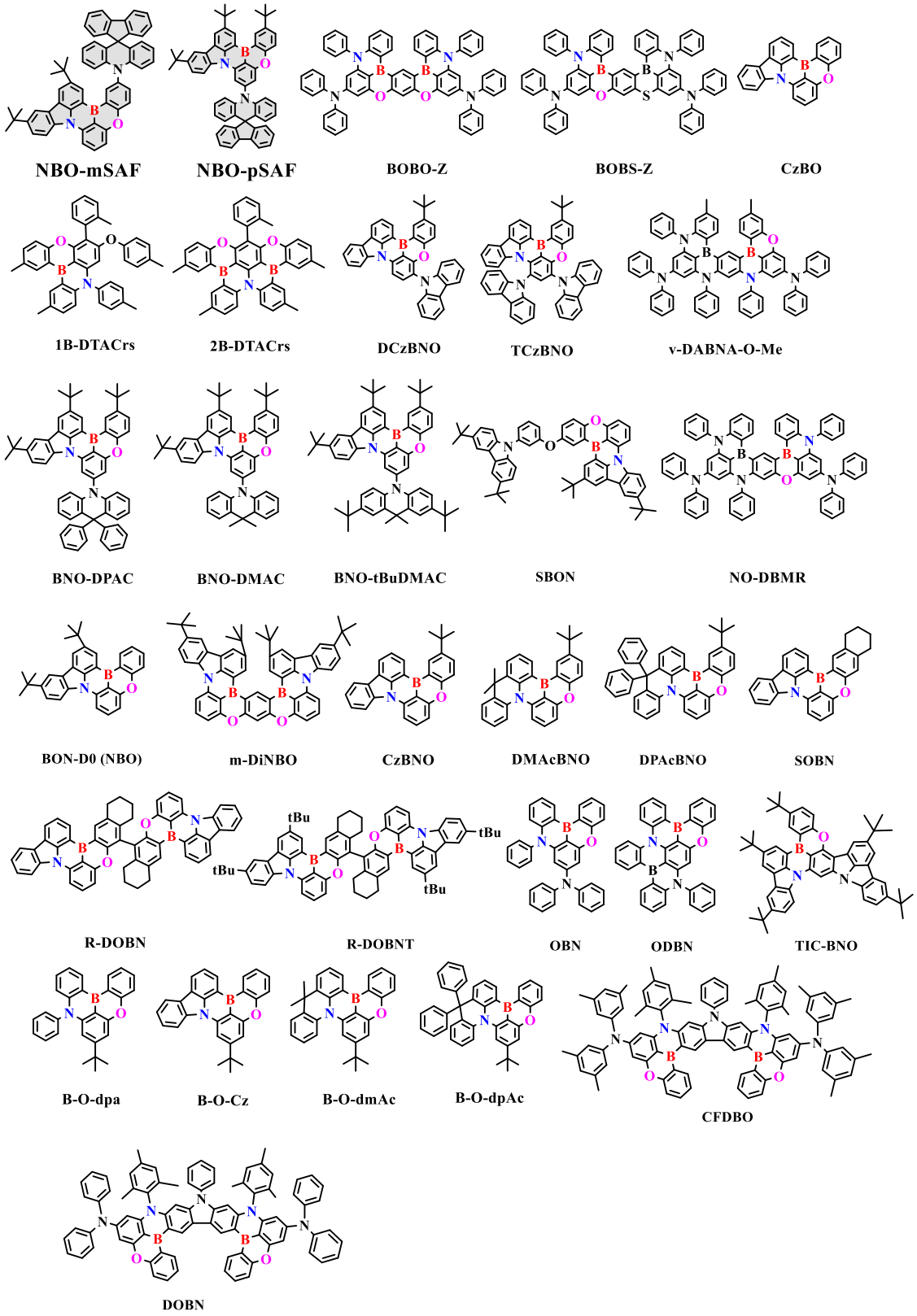

Figure S1. Molecular structure of the blue MR-TADF emitters with N/B/O structure.

Table S1. EL properties of the blue MR-TADF emitters with N/B/O structure.

Emitter	Device type	λ_{EL} [nm]	FWHM [nm]	EQE_{max} [%]	CIE [x,y]	Ref
NBO-mSAF		**466**	**28**	**29.5**	**0.128,0.114**	**This work**
NBO-pSAF		**451**	**26**	**20.5**	**0.147,0.048**	**This work**
BOBO-Z		445	18	13.6	0.15,0.04	1
CzBO		448	30	13.4	0.15,0.05	2
B-O-dpa		443	32	16.3	0.15,0.05	3
1B-DTACrs		440	30	1.31	0.154,0.049	4
2B-DTACrs		447	26	14.8	0.150,0.044	
DOBN		449	20	24.14	0.15,0.04	5
BNO-DPAC	HF	448	36	27.7	0.151,0.083	
BNO-DMAC	HF	449	36	28.7	0.149,0.090	6
BNO-tBuDMAC	HF	447	59	27.7	0.155,0.144	
DCzBNO	HF	469	45	31.7	0.13,0.15	7
TCzBNO	HF	482	52	36.5	0.13,0.25	
v-DABNA-O-Me		465	23	29.5	0.13,0.10	8
BOBS-Z		456	23	26.9	0.14,0.06	1
SBON		466	28	13.7	0.13,0.13	9
BON-D0	Solution-processed	460	39	9.7	0.14,0.12	10
NBO		459	45	16.8	0.137,0.142	11
m-DiNBO		466	21	24.2	0.126,0.098	
CzBNO		454	36	13.6	0.14,0.08	
DMAcBNO		472	41	20.4	0.13,0.19	12
DPAcBNO		468	37	23.0	0.13,0.14	
SOBN		460	47	14.6	0.14,0.14	
R-DOBN		459	38	23.9	0.14,0.10	13
R-DOBN-T		464	35	25.6	0.13,0.12	
B-O-Cz		481	63	13.4	0.13,0.22	
B-O-dmAc		475	44	16.2	0.12,0.21	3
B-O-dpAc		473	42	17.0	0.12,0.20	
OBN		437	44	15.7	0.15,0.09	14
ODBN		446	54	24.15	0.147,0.099	

Emitter	Device type	λ_{EL} [nm]	FWHM [nm]	EQE_{max} [%]	CIE [x,y]	Ref
NO-DBMR		469	26	33.7	0.12,0.12	[15]
TIC-BNO		476	38	34.58	0.123,0.222	[16]
CFDBO		469	24	20.7	0.14,0.12	[17]

2. Experimental Section

General information

The ^{1}H NMR spectra were measured on a 400 MHz Bruker Avance II 400 using $CDCl_3$ as the solvent. Tetramethyl silane (TMS) was used as an internal reference. The ^{13}C NMR spectra were recorded by AVANCENEO 500 M using Chloroform-d ($CDCl_3$) as the solvent. The mass spectra were recorded by HP1100LC/MSD MS spectrometer and matrix-assisted laser desorption/ionization (MALDI) micro mass spectrometry (MS) spectrometer. The ultraviolet-visible (UV-Vis) absorption spectra were recorded on a Perkin-Elmer Lambda 750S spectrophotometer. Fluorescence spectra and transient photoluminescence (PL) decay at room temperature were measured with an Edinburgh FLS1000 fluorescence spectrometer. Low temperature phosphorescence spectra were measured on a Hitachi F-7000 fluorescence spectrometer at 77 K in toluene. Cyclic voltammetry (CV) curves were achieved with a CHI610E electrochemical work station, with glass-carbon as the working electrode, a saturated calomel electrode (SCE) as reference electrode and a Pt wire as counter-electrode. Oxidation and reduction curves were obtained in the 0.1 M solutions in dichloromethane (DCM) and dimethylformamide (DMF), respectively with n-Bu_4NPF_6 as the supporting electrolyte. Absolute photoluminescence quantum yields (PLQYs) of the compounds were measured in doped films on a HAMAMATSU absolute PL quantum yield spectrometer (C11347).

The Lippert-Mataga calculation

The effect of solvent polarity on photophysical properties of **NBO-mSAF** and **NBO-pSAF** was analyzed by the Lippert-Mataga equation [18]:

(S1) $$\boldsymbol{hc(\nu_a - \nu_f) = hc(\nu_a^0 - \nu_f^0) + \frac{2(\mu_e-\mu_g)^2}{a_0^3} f\ (\varepsilon, n)}$$

According to the equation S1, we got

(S2) $$\boldsymbol{\mu_e = \mu_g + \left\{\frac{hca_0^3}{2} \cdot \left[\frac{d(\nu_a-\nu_f)}{df\ (\varepsilon,n)}\right]\right\}^{1/2}}$$

Where ν_a and ν_f represent wavenumbers of maximal absorption and emission, respectively; h is the Plank constant; c is the light speed in vacuum; (ν_a - ν_f) is the Stokes shift; (ν_a^0-ν_f^0) corresponds to the Stokes shift at $f(\varepsilon, n)$=0; μ_e is the excited-state dipole; μ_g is the ground-state dipole moment that can be estimated by DFT calculations (2.36 and 2.92 D for **NBO-mSAF** and **NBO-pSAF**, respectively); a_0 is the solvent cavity (Onsager) radius and $f(\varepsilon, n)$ is the orientational polarizability of the solvent. a_0 and $f(\varepsilon, n)$ can be calculated as follows:

(S3) $$\boldsymbol{a_0 = \sqrt[3]{\frac{3M}{4N\pi d}}}$$

Where N is the Avogadro number; M is the molecular weight and d is the density (d = 1.0 g cm^{-3}).

(S4) $$\boldsymbol{f\ (\varepsilon, n) = \frac{\varepsilon-1}{2\varepsilon+1} - \frac{n^2-1}{2n^2+1}}$$

Where ε is the solvent dielectric constant and n is solvent refractive index.

Kinetic parameters calculation of photophysical processes

The prompt fluorescence lifetimes (τ_{PF}) were determined by time correlated single photon counting (TCSPC) method with a 375 nm picosecond pulsed LED as the excitation source at room temperature. And delayed fluorescence lifetimes (τ_{DF}) were measured using multi-channel scaling (MCS) as data acquisition technique with a 365 nm variable pulsed LED as the excitation source and at room temperature. The lifetimes were calculated using the following equations:

(S5) $$\boldsymbol{\tau} = \frac{B_1\tau_1^2+B_2\tau_2^2+B_3\tau_3^2}{B_1\tau_1+B_2\tau_2+B_3\tau_3}$$

The equations used to calculate the excited state kinetics parameters are as follows.

(S6) $$\boldsymbol{k_p = 1 / \tau_{PF}}$$

(S7) $$\boldsymbol{k_d = 1 / \tau_{DF}}$$

(S8) $$\boldsymbol{k_r = \Phi_{PF} / \tau_{PF}}$$

(S9) $$\boldsymbol{\Phi_{PL} = k_r / (k_r + k_{nr})}$$

(S10) $$\boldsymbol{\Phi_{PF} = k_r / (k_r + k_{ISC} + k_{nr})}$$

(S11) $$\boldsymbol{k_{RISC} = k_p\, k_d\, \Phi_{DF} / k_{ISC}\, \Phi_{PF}}$$

k_p and k_d represent the rate constants of prompt process and delay process, while k_r and k_{nr} represent the rate constants of radiation and non-radiation. k_{ISC} and k_{RISC} represent rate constants of intersystem crossing and reverse intersystem crossing, respectively. Φ_{PL}, Φ_{PF} and Φ_{DF} represent total PLQY, quantum yield of the prompt component and quantum yield of the delayed component, respectively. τ_{PF} and τ_{DF} represent average lifetimes of the prompt and delayed components, respectively.

Theoretical calculations

The theoretical calculations were performed with the Gaussian 16 package, using the density functional theory (DFT) and time-dependent density functional theory (TDDFT) method with the M062X hybrid functional. The ground states (S_0) geometries and the lowest excited singlet and triplet states geometries (S_1 and T_1) were optimized through DFT/TD-DFT methods at the M062X/def2svp level in the gas phase. The related HOMO and LUMO orbitals, and the natural transition orbitals (NTOs) were analyzed and then plotted through Multiwfn 3.8 and VMD.[19] The spin-orbit coupling (SOC) between S_n (n = 1,2) and T_n (n = 1-6) states were calculated with PySOC at the TD-DFT level of theory using the M062X functional and the def2zvp basis set with PySOC.

Devices fabrication

The involved functional layer materials except for emitters were gained through commercial sources. The ITO glass substrates with a certain resistance were cleaned in different detergents, and handled in ozone atmosphere for 30 min. For all the devices, the functional layer materials were fabricated with a pressure below 1×10^{-4} Pa. Each device possesses an effective light-emitting area of 3.0×3.0 mm^2. Current density-voltage-luminance (*J-V-L*) curves and electroluminescence (EL) spectra were recorded on Keithley 2400 SMU and a Konica Minolta Chroma Meter CS-200 and HAMAMATSU C9920-11, respectively. All relevant device measurements were operated in the air without further encapsulations. The forward viewing external quantum efficiency was calculated by using the current efficiency, EL spectra and human photopic sensitivity.

3. Syntheses

General procedure for syntheses of NBO-mBr and NBO-pBr

NBO-pBr was synthesized following the literature method.[6] **NBO-mBr** was prepared according to the procedure in Scheme S1.

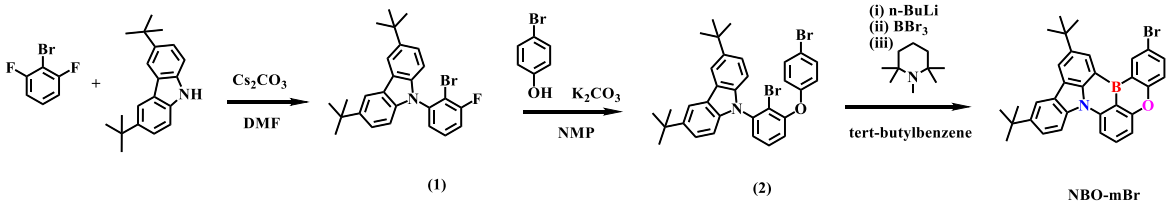

Scheme S1. Synthesis of **NBO-mBr**.

9-(2-bromo-3-fluorophenyl)-3,6-di-tert-butyl-9H-carbazole (1): A mixture of 2-bromo-1,3-difluorobenzene (10.0 g, 51.8 mmol), 3,6-di-tert-butyl-9H-carbazole (12.8 g，45.8 mmol), and Cs_2CO_3 (27.2 g, 83.3 mmol) in dry DMF (150 mL) was stirred at 150 ℃ for 12 h. After cooling to room temperature, the reaction mixture was added into a large amount of water and then extracted with CH_2Cl_2. The combined organic layer was washed with water and dried over anhydrous Na_2SO_4. After filtration and evaporation, the crude product was purified by column chromatography to yield intermediate (**1**), which was put into the following reaction without characterization.

9-(2-bromo-3-(4-bromophenoxy)phenyl)-3,6-di-tert-butyl-9H-carbazole (2): A mixture of compound (**1**) (10.0 g, 22.1 mmol), 4-bromophenol (10.4 g, 60.2 mmol) and K_2CO_3 (8.3 g, 60.1 mmol) was dissolved in anhydrous N-methylpyrrolidinone (120 mL). The mixture was stirred at 180 ℃ under a nitrogen atmosphere for 24 h. After cooling to room temperature, the reaction mixture was poured into ice water and the precipitate was filtered and washed with water. The crude product was extracted with toluene and dried over $MgSO_4$, and purified by column chromatography. **(2):** ^{1}H NMR (400 MHz, $CDCl_3$) δ 8.62 (s, 2H), 8.00 – 7.84 (m, 5H), 7.73 – 7.68 (m, 1H), 7.55 (d, *J* = 8.1 Hz, 1H), 7.49 (d, *J* = 8.0 Hz, 2H), 7.42 (d, *J* = 8.9 Hz, 2H), 1.93 (d, *J* = 1.5 Hz, 18H).

NBO-mBr: To a solution of compound **(2)** (2.5 g, 4.1 mmol) in dry tert-butylbenzene (200 mL) was slowly added n-BuLi (2.5 M solution in hexane, 2.0 mL, 5.0 mmol) at -20 ℃. After reacting for 2 h at room temperature, BBr_3 (0.6 mL, 6.2 mmol) was slowly added at -20 ℃, and then the mixture was stirred at room temperature for 2 h. After addition of 1,2,2,6,6-pentamethylpiperidine (2.9 mL, 16.5

mmol) at 0 ℃, the reaction mixture was further stirred at 130 ℃ for 14 h. After cooling to room temperature, the reaction mixture was carefully quenched by adding methanol, then the solvent was removed in vacuo. The mixture was extracted with dichloromethane and the organic phase was washed with water. After removing dichloromethane, and mixture was purified by column chromatography to give pure **NBO-mBr:** ^{1}H NMR (500 MHz, $CDCl_3$) δ 8.81 (d, *J* = 2.5 Hz, 1H), 8.74 (s, 1H), 8.42 (s, 1H), 8.25 (d, *J* = 8.7 Hz, 1H), 8.20 – 8.11 (m, 2H), 7.85 (t, *J* = 8.2 Hz, 1H), 7.69 (dd, *J* = 8.6, 2.4 Hz, 1H), 7.59 (dd, *J* = 8.7, 2.1 Hz, 1H), 7.36 (d, *J* = 8.9 Hz, 1H), 7.21 (s, 1H), 1.57 (s, 9H), 1.45 (s, 9H).

General procedure for syntheses of NBO-mSAF and NBO-pSAF

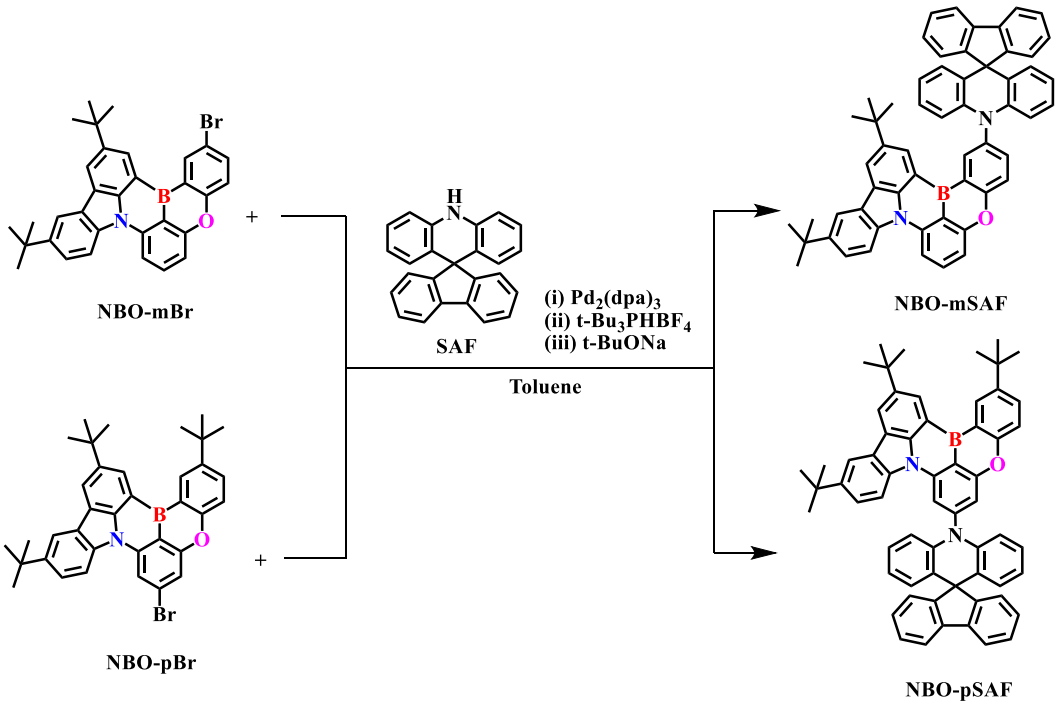

Scheme S2. Synthesis of **NBO-mSAF** and **NBO-pSAF**.

A mixture of **NBO-mBr** (500.0 mg, 0.9 mmol) or **NBO-pBr** (500.0 mg, 0.9 mmol), 10H-spiro[acridine 9,9'-fluorene] (0.8 mmol), $Pd_2(dba)_3$ (46.0 mg, 0.05 mmol), t-Bu_3PHBF_4 (32.0 mg, 0.1 mmol), t-BuONa (167 mg, 1.7 mmol) and 50 mL anhydrous toluene in a prewired 100 mL flask was stirred at 110℃ under nitrogen atmosphere for 12 h. After the confirmation of TLC tracking reaction, the solvent was removed by vacuum distillation. The mixture was extracted with dichloromethane and

the organic phase was washed with water. After the dichloromethane was removed, the mixture was purified by column chromatography (PE: DCM = 10:1) to obtain the crude product and finally recrystallized from CH_2Cl_2/methanol to give the yellow powder as pure product.

NBO-mSAF: yield 45.2%. ^{1}H NMR (400 MHz, $CDCl_3$) δ 8.96 (s, 1H), 8.85 (s, 1H), 8.52 (s, 1H), 8.40 (d, *J* = 8.8 Hz, 1H), 8.31 (t, *J* = 8.3 Hz, 2H), 8.02 (t, *J* = 8.2 Hz, 1H), 7.92 (d, *J* = 8.6 Hz, 1H), 7.79-7.89 (m, 3H), 7.71 (d, *J* = 8.8 Hz, 1H), 7.55 (d, *J* = 7.5 Hz, 2H), 7.44 (t, *J* = 7.8 Hz, 3H), 7.34 (t, *J* = 7.4 Hz, 2H), 7.02 – 6.94 (t, *J* = 8.8 Hz, 2H), 6.68 – 6.57 (m, 4H), 6.50 (d, *J* = 7.8 Hz, 2H), 1.58 (s, 9H), 1.55 (s, 9H). ^{13}C NMR (126 MHz, $CDCl_3$) δ 159.14, 159.05, 156.68, 145.70, 144.95, 142.44, 142.02, 141.78, 139.33, 138.22, 137.34, 136.03, 135.52, 134.42, 129.06, 128.49, 127.82, 127.64, 127.34, 126.80, 125.78, 125.00, 124.75, 124.25, 121.75, 121.04, 120.72, 119.98, 117.32, 114.89, 114.04, 109.02, 107.79, 77.30, 77.05, 76.79, 56.99, 35.11, 34.85, 32.10, 31.84, 1.05, 0.03. MALDI-HRMS ($C_{57}H_{45}BN_2O$, *m/z*): $[M]^+$ calculated: 784.3625, found: 784.3605.

NBO-pSAF: yield 47.8%. ^{1}H NMR (400 MHz, $CDCl_3$) δ 9.09 (s, 1H), 9.00 (s, 1H), 8.55 (s, 1H), 8.36 (s, 1H), 8.31(t, *J* = 7.1 Hz, 2H), 7.87 (d, *J* = 7.1 Hz, 3H), 7.68 – 7.55 (m, 4H), 7.51 (s, 1H), 7.45 (t, *J* = 7.4 Hz, 2H), 7.37 (t, *J* = 7.4 Hz, 2H), 7.00 – 6.91 (t, *J* = 6.9 Hz, 2H), 6.65 (dd, J = 14.1, 7.7 Hz, 4H), 6.51 (d, *J* = 7.8 Hz, 2H), 1.70 (s, 9H), 1.59 (s, 9H), 1.52 (s, 9H). ^{13}C NMR (126 MHz, $CDCl_3$) δ 161.50, 157.95, 156.46, 146.35, 145.97, 145.45, 145.23, 144.40, 142.25, 141.09, 139.35, 138.03, 131.53, 130.75, 129.73, 128.49, 127.81, 127.72, 127.50, 126.93, 125.93, 125.07, 124.91, 124.30, 121.54, 120.91, 120.02, 118.74, 117.57, 117.32, 114.95, 114.07, 111.31, 109.84, 77.31, 77.05, 76.80, 56.96, 35.26, 34.86, 34.70, 32.18, 31.81, 31.66, 1.07, 0.04. MALDI-HRMS ($C_{61}H_{53}BN_2O$, *m/z*): $[M]^+$ calculated: 840.4251, found: 840.4251.

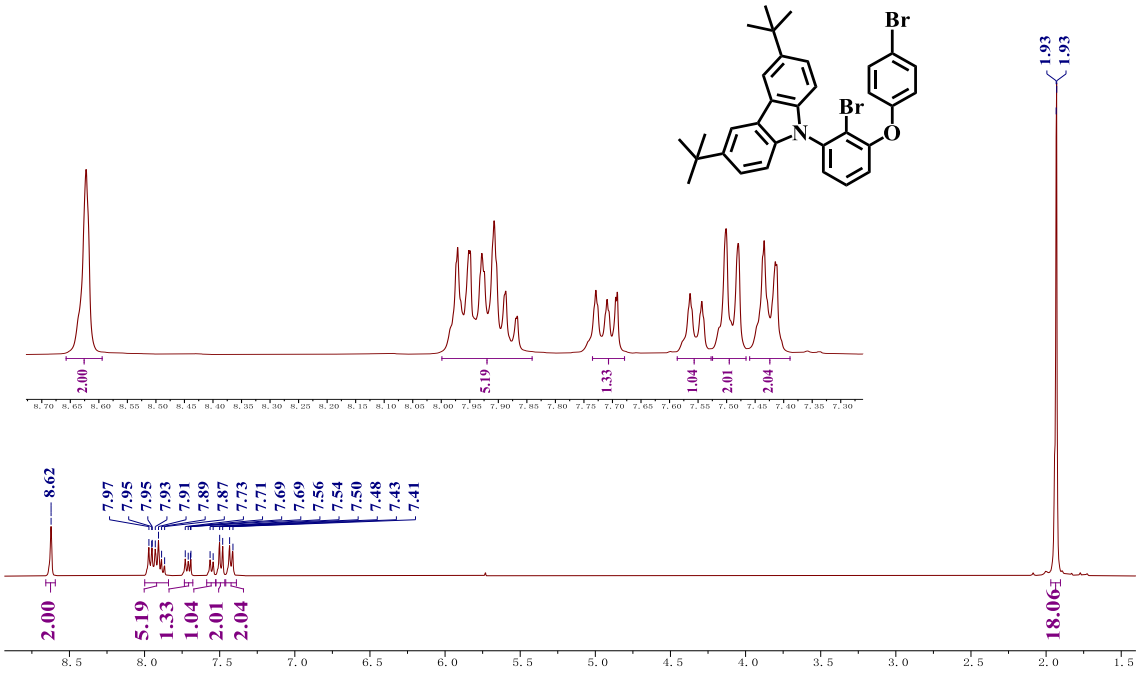

Figure S2. ^{1}H NMR spectrum of **compound (2)**.

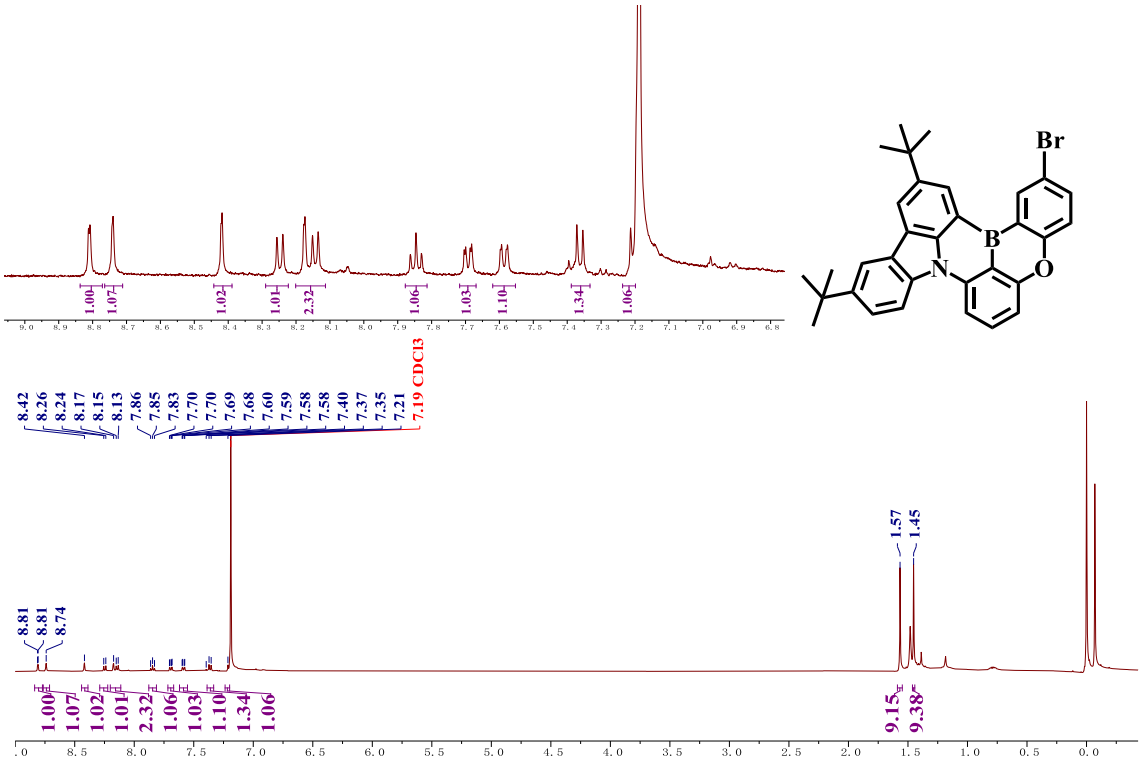

Figure S3. ^{1}H NMR spectrum of **NBO-mBr**.

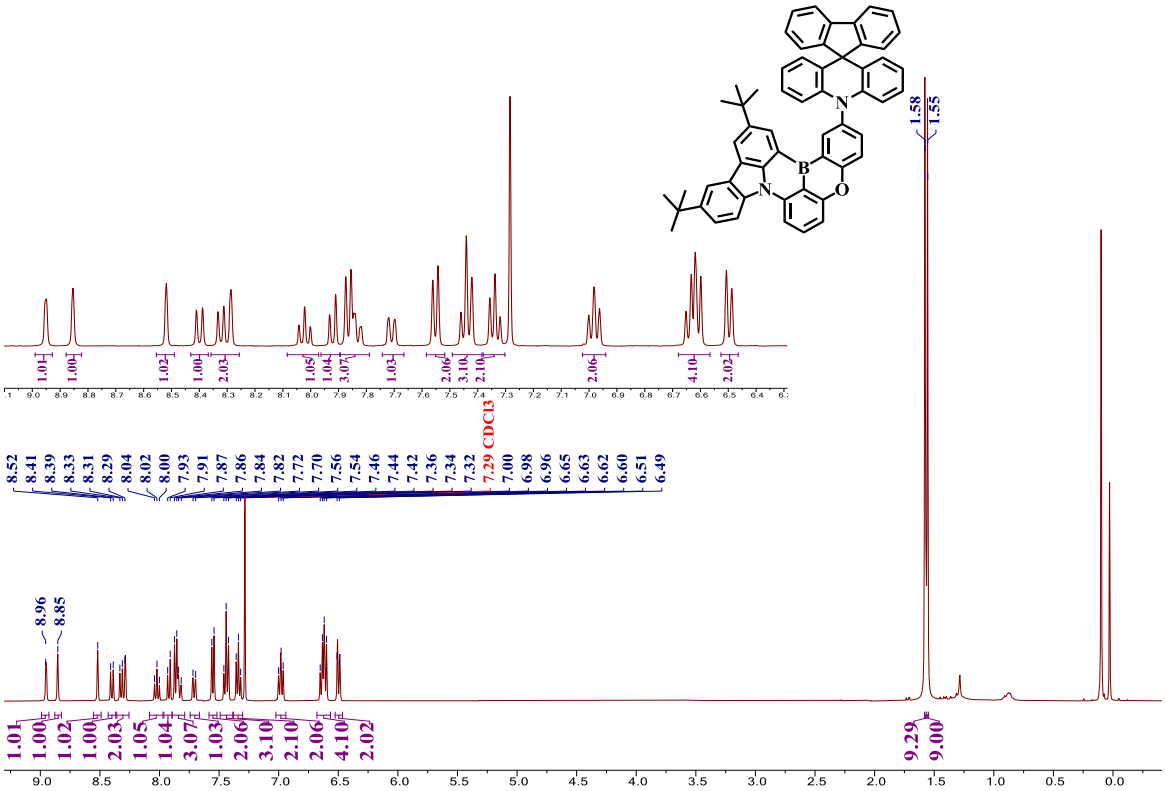

Figure S4. ^{1}H NMR spectrum of **NBO-mSAF**.

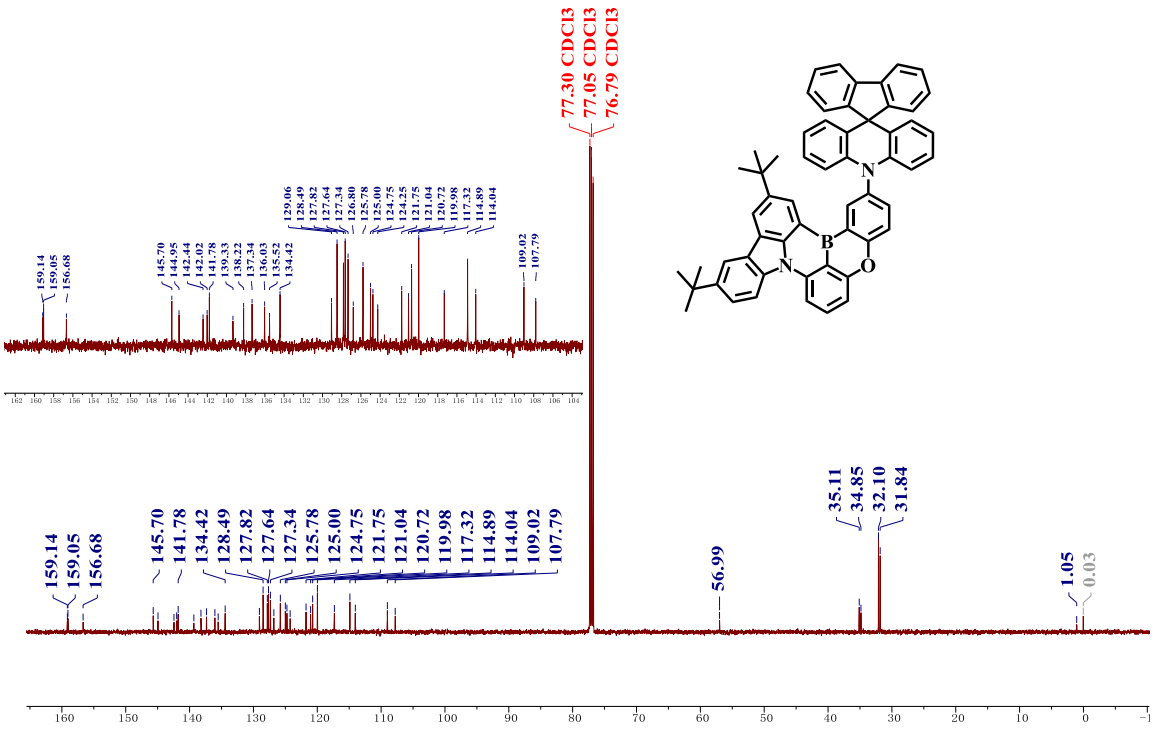

Figure S5. ^{13}C NMR spectrum of **NBO-mSAF**.

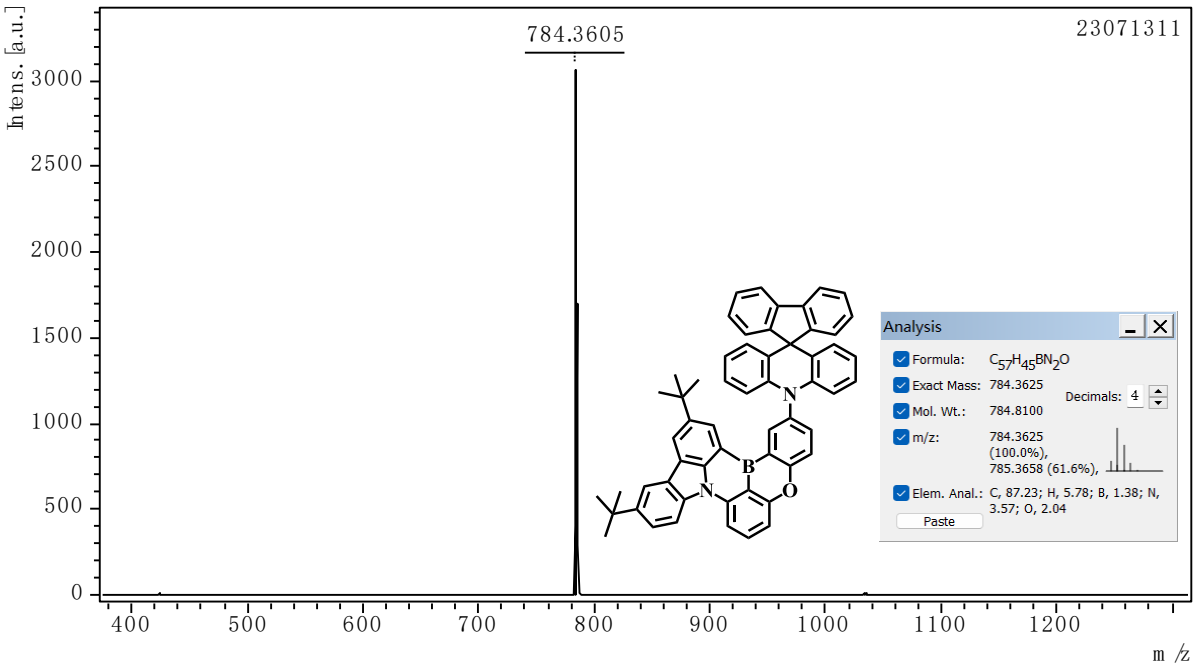

Figure S6. Mass spectrum of **NBO-mSAF**.

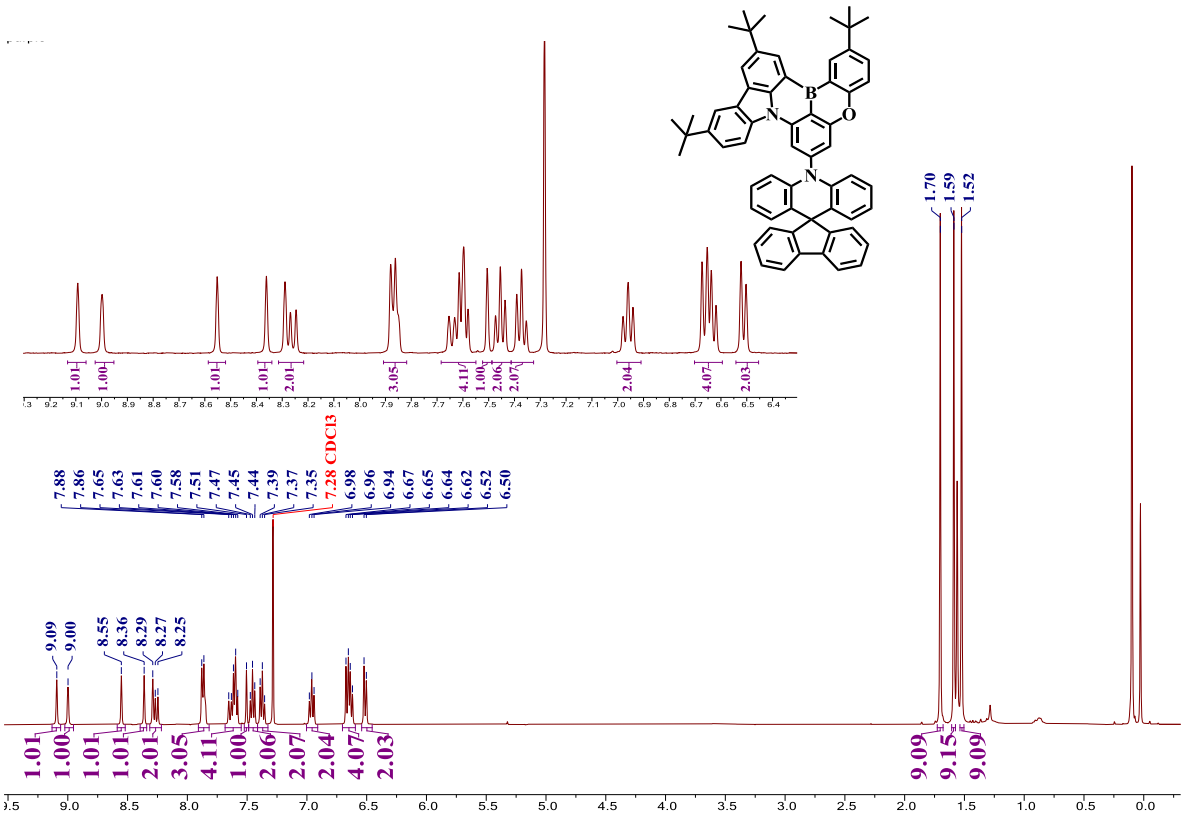

Figure S7. ^{1}H NMR spectrum of **NBO-pSAF**.

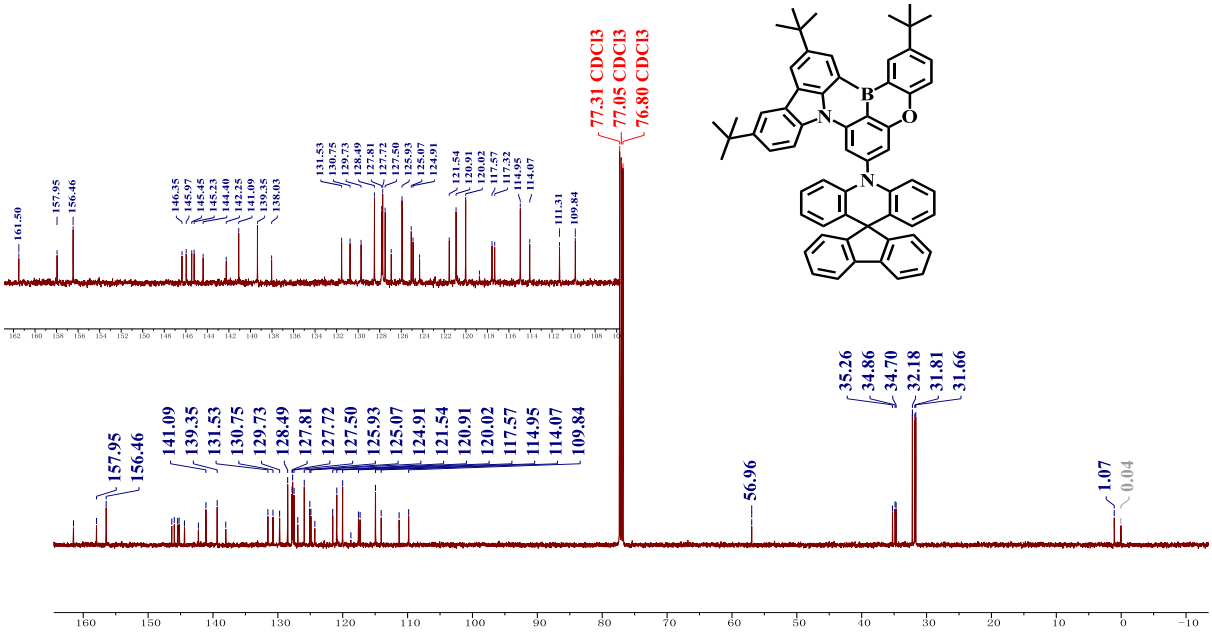

Figure S8. ^{13}C NMR spectrum of **NBO-pSAF**.

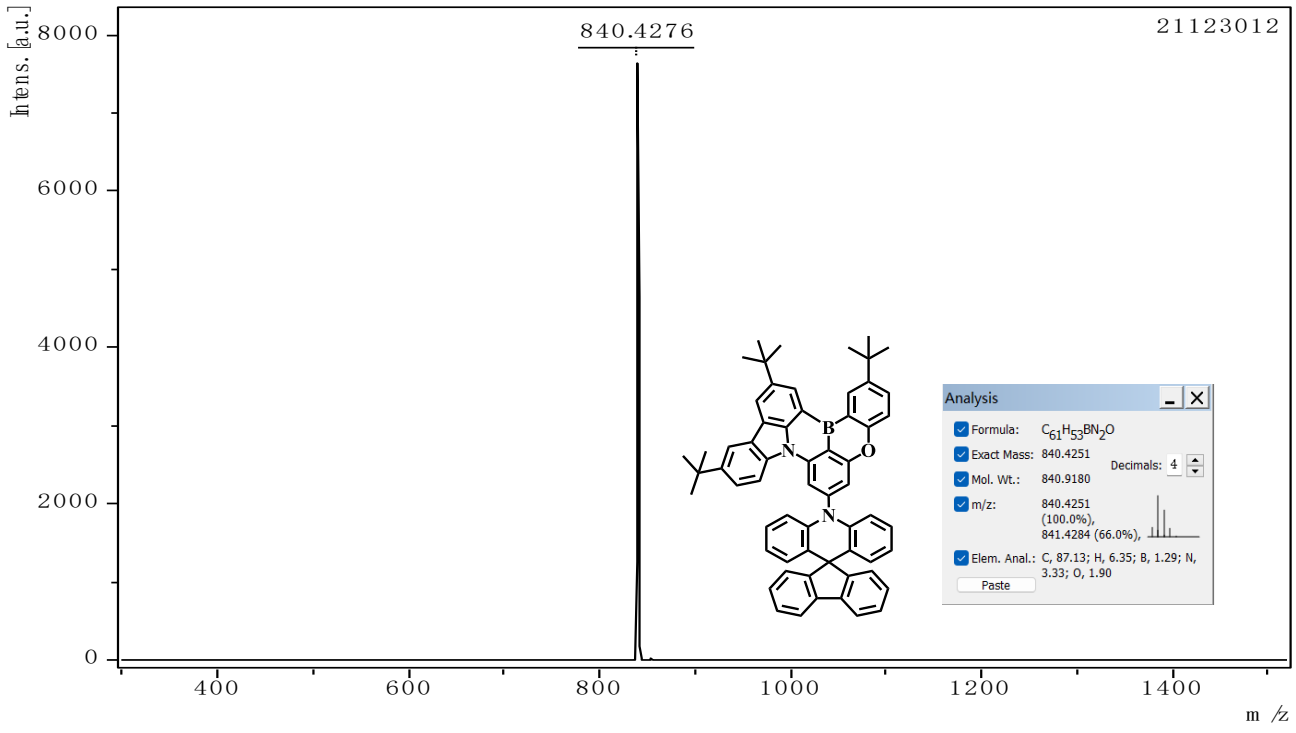

Figure S9. Mass spectrum of **NBO-pSAF**.

4. Supplementary figures

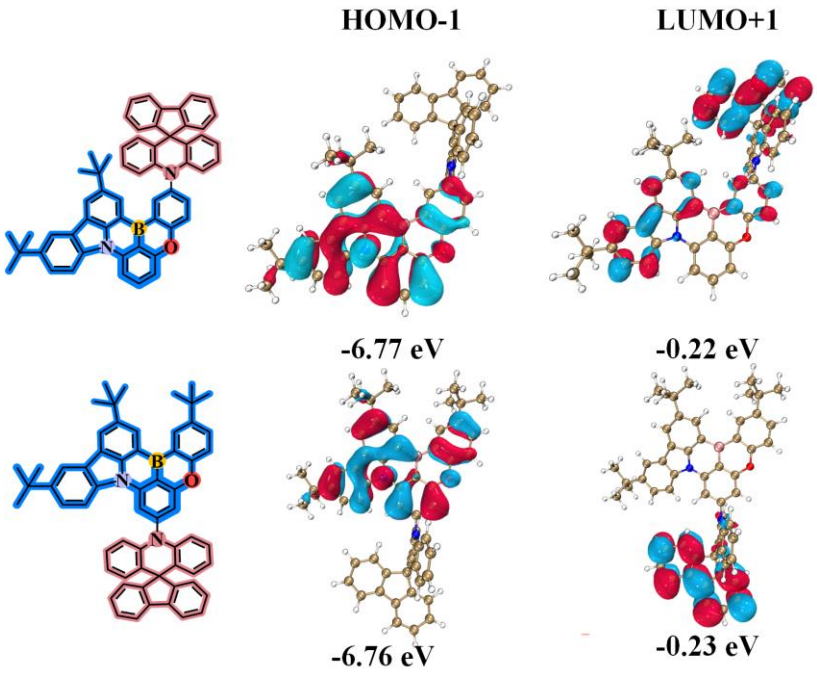

Figure S10. Orbital distribution and energy levels of HOMO-1 and LUMO+1 of **NBO-mSAF** and **NBO-pSAF**.

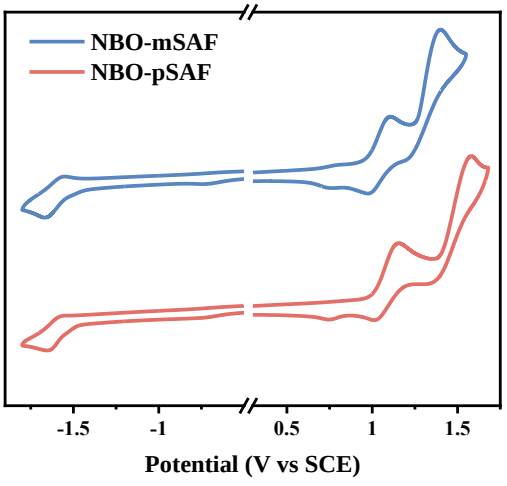

Figure S11. Cyclic voltammograms of **NBO-mSAF** and **NBO-pSAF** in dilute DCM (anodic) and DMF (cathodic) solutions.

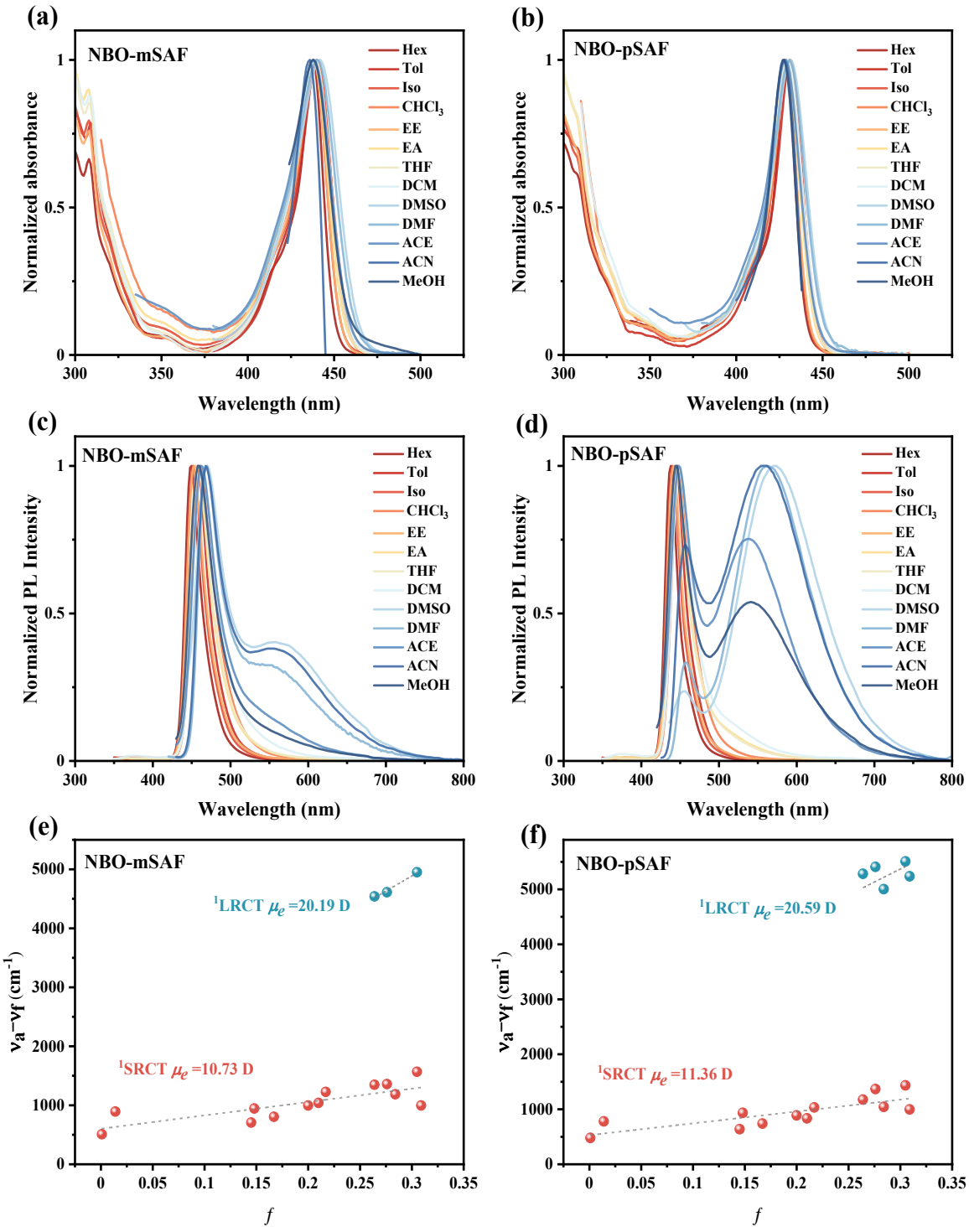

Figure S12. The absorption spectra (a, b), emission spectra (c, d) of **NBO-mSAF** and **NBO-pSAF** in different polar solvents and the linear relationship between solvent oriented polarizability (f) and Stokes shift ($\nu_a - \nu_f$) (e, f).

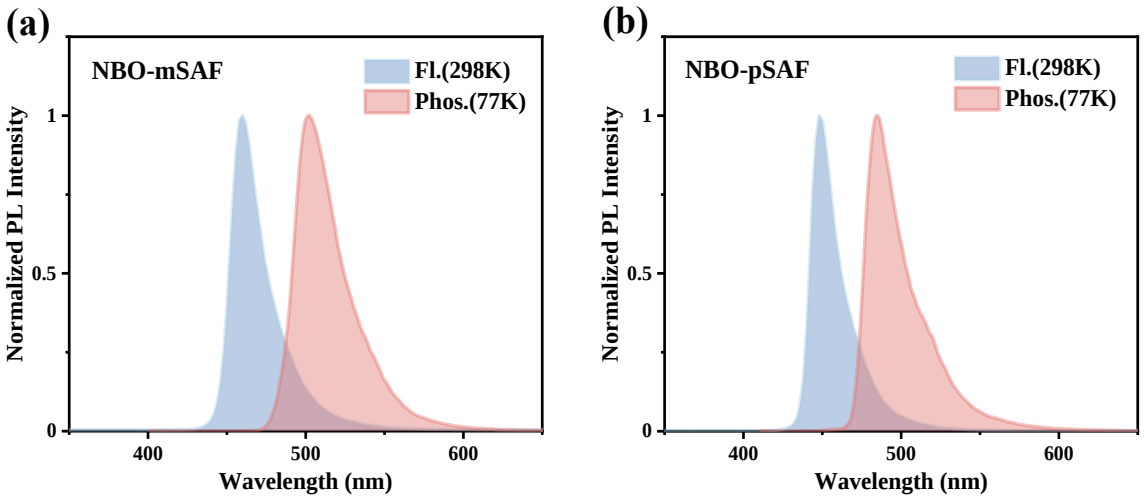

Figure S13. Fluorescence (300K) and phosphorescence (77K) spectra of (a) **NBO-mSAF** and (b) **NBO-pSAF** in dilute 2-MeTHF solution.

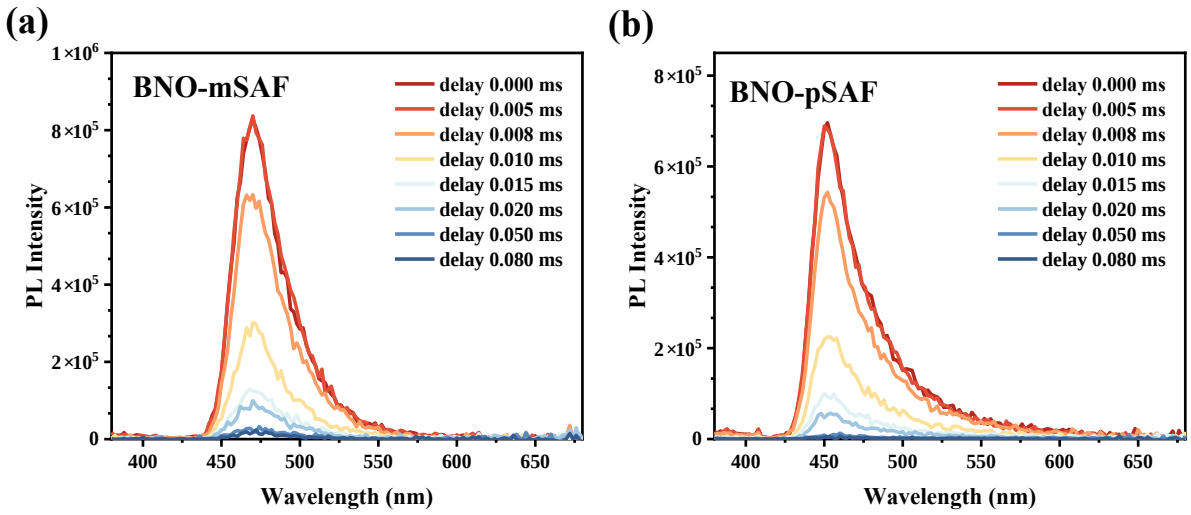

Figure S14. The prompt and delayed emission spectra for (a) **NBO-mSAF** and (b) **NBO-pSAF** in doped films (6 wt% in 26DCzPPy host).

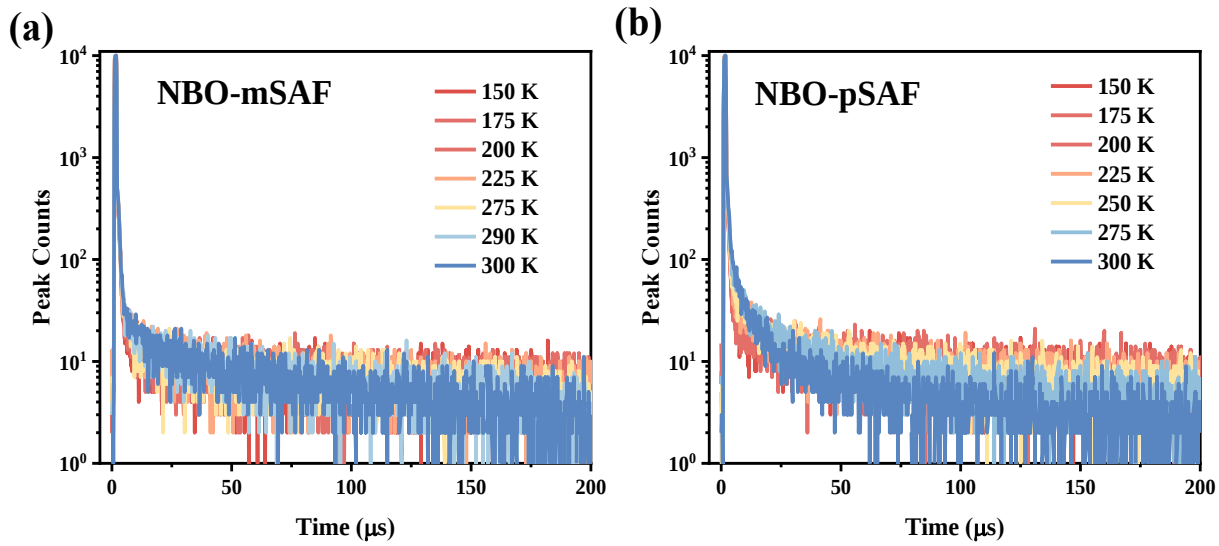

Figure S15. Temperature dependent transient PL decay curves for (a) **NBO-mSAF** and (b) **NBO-pSAF** in doped films (6 wt% in 26DCzPPy host).

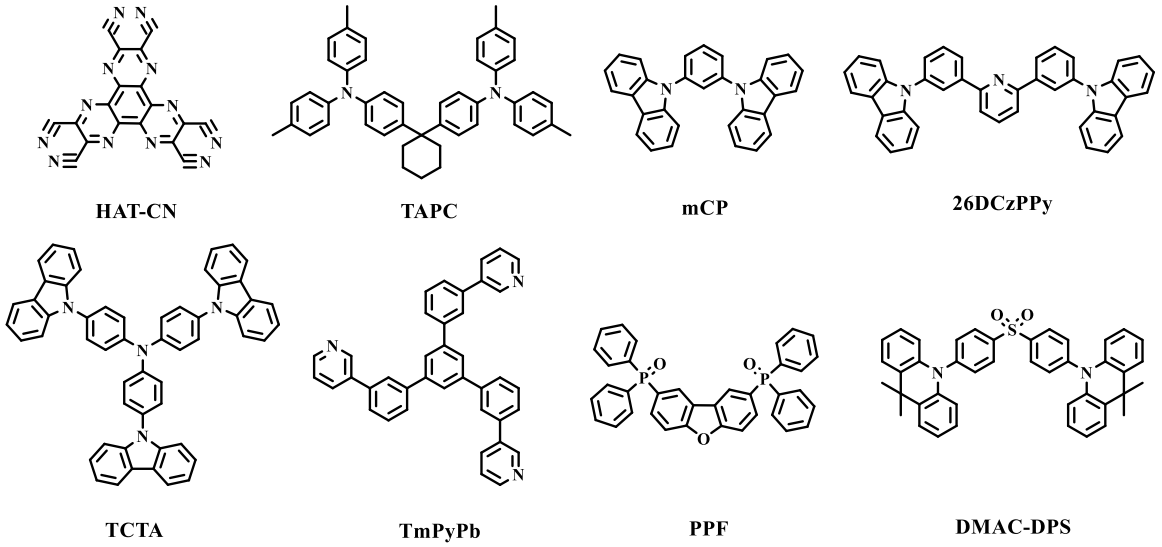

Figure S16. Chemical structures of the materials utilized in present OLED fabrication.

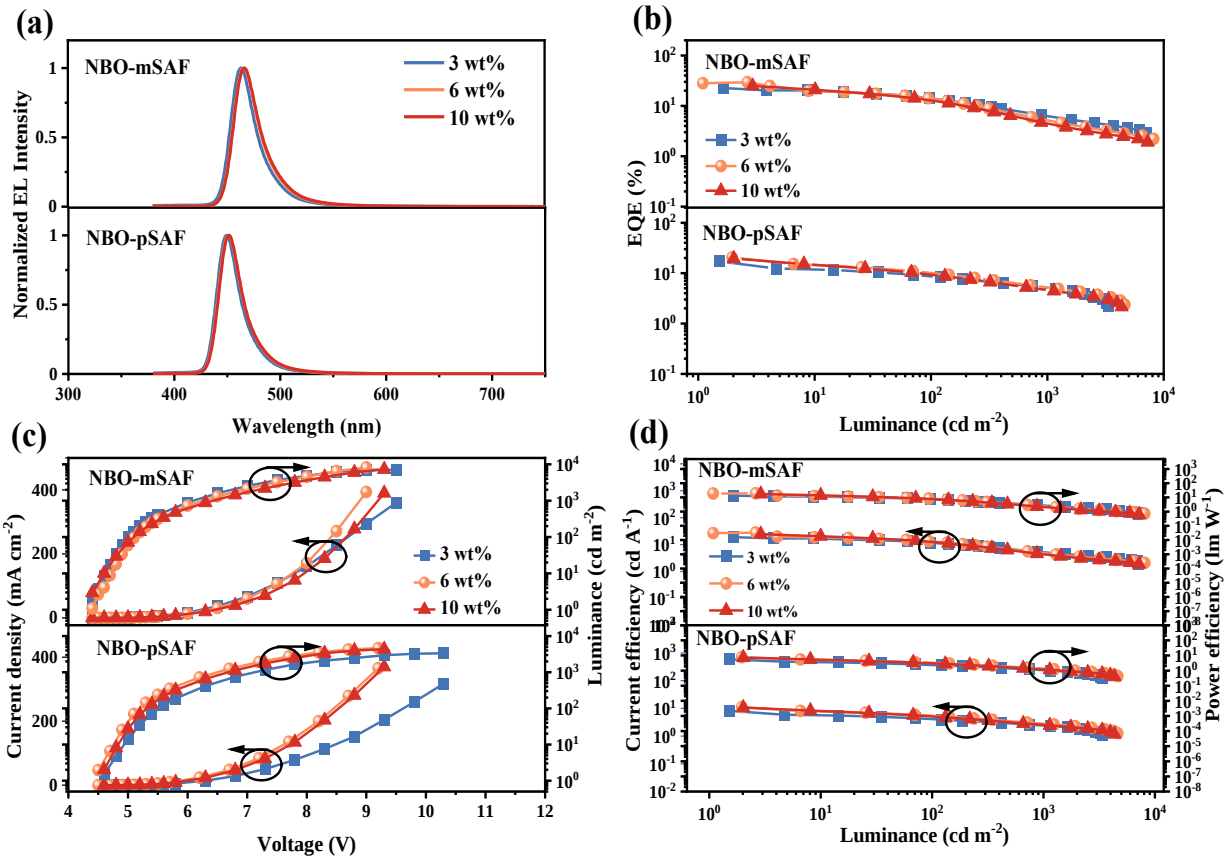

Figure S17. Doping concentration optimization for **NBO-mSAF** and **NBO-pSAF** devices with 26DCzPPy as host. (a) EL spectra; (b) EQE-Luminance curves; (c) Current density-voltage-luminance; (d) Current efficiency-luminance-Power efficiency curves.

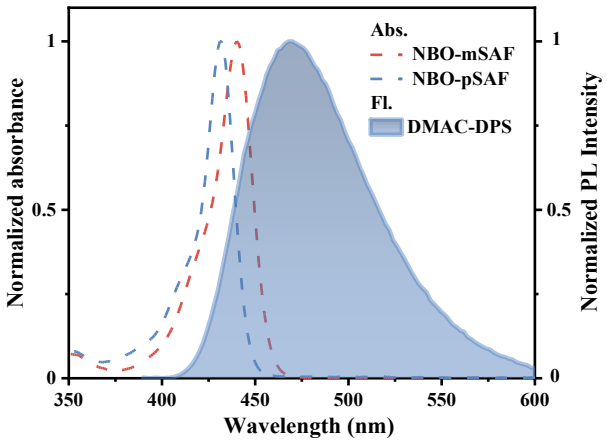

Figure S18. Comparison between fluorescence spectra (Fl., measured at 300 K) of the sensitizer (DMAC-DPS) and UV-vis absorption spectra (Abs., measured at 300 K) of the emitters in toluene solution.

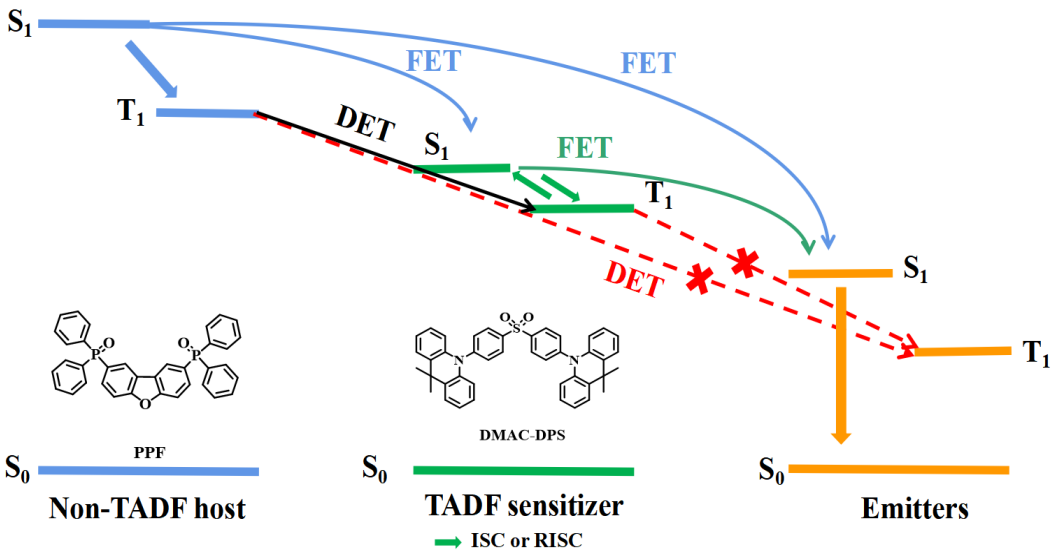

Figure S19. The energy transfer process for HF-devices.

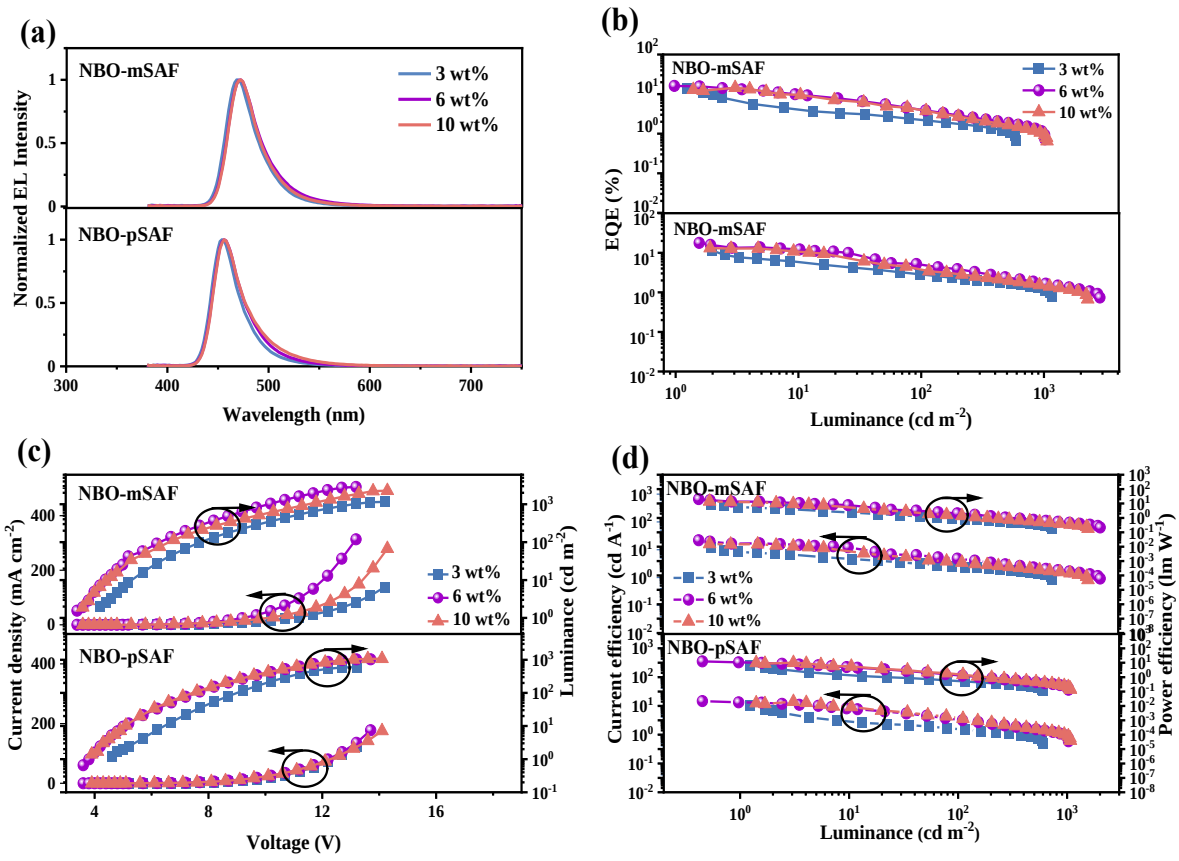

Figure S20. Electroluminescent performance of the sensitizer-free devices at different doping concentrations in PPF host. (a) EL spectra; (b) EQE-Luminance curves; (c) Current density-voltage-luminance; (d) Current efficiency-luminance-Power efficiency curves.

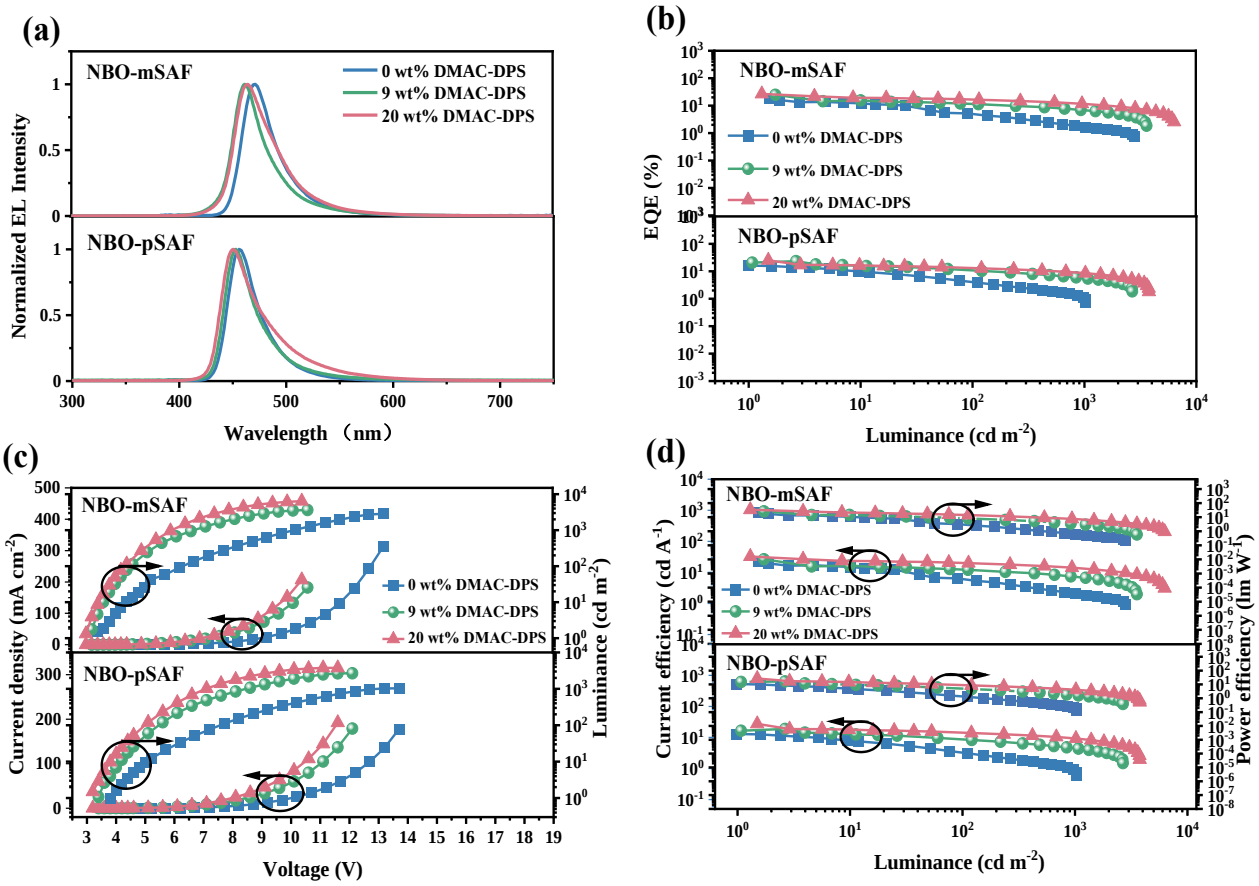

Figure S21. Electroluminescent performance of sensitizer at different doping concentrations (sensitizer: DMAC-DPS). (a) EL spectra; (b) EQE-Luminance curves; (c) Current density-voltage-luminance; (d) Current efficiency-luminance-Power efficiency curves.

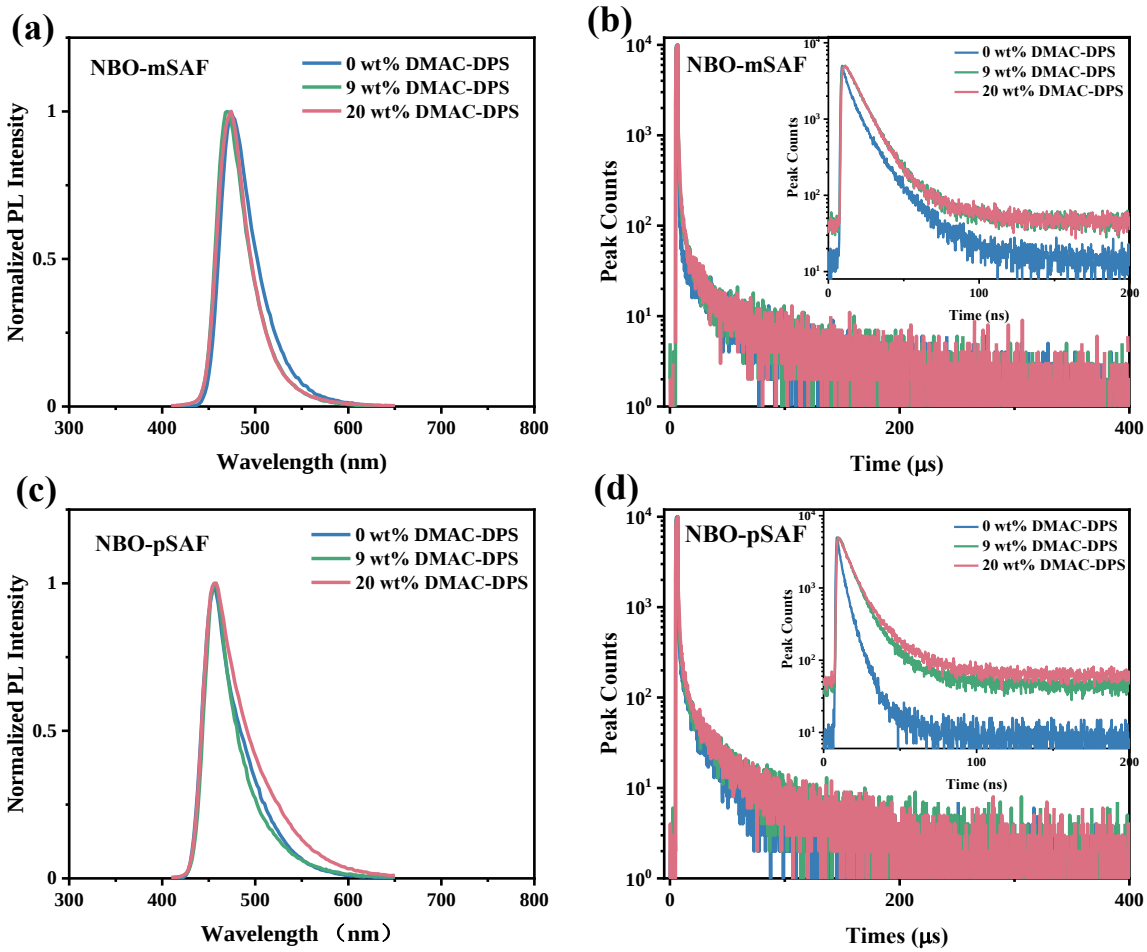

Figure S22. The normalized PL spectra (a, c) and transient photoluminescence decay curves (b, d) of sensitizer at different doping concentrations (sensitizer: DMAC-DPS) of **NBO-mSAF** and **NBO-pSAF**.

5. Supplementary tables

Table S2. Summary of TD-DFT data for **NBO-mSAF** and **NBO-pSAF** at M062X/def2svp level.

Compound	Transition	Wavelength (nm)	Energy (eV)	Oscillator Strength	Coefficient of Orbital
NBO-mSAF	S_0-S_1	355	3.49	0.3859	HOMO-1→LUMO (92.4%)
	S_0-S_2	336	3.68	0.0031	HOMO→LUMO (86.3%)
	S_0-T_1	422	2.94	0.0000	HOMO-1→LUMO (88.2%)
	S_0-T_2	377	3.29	0.0000	HOMO-3→LUMO (64.1%) HOMO-3→LUMO+2 (16.3%) HOMO-3→LUMO+1 (6.1%)
	S_0-T_3	350	3.53	0.0000	HOMO-2→LUMO+1 (54.9%) HOMO-2→LUMO+2 (17.9%) HOMO-4→LUMO+1 (5.3%)
	S_0-T_4	345	3.59	0.0000	HOMO→LUMO (50.8%) HOMO→LUMO+4 (10.9%) HOMO-5→LUMO (5.9%)
NBO-pSAF	S_0-S_1	353	3.51	0.3691	HOMO-1→LUMO (94.6%)
	S_0-S_2	340	3.65	0.0170	HOMO→LUMO (82.4%) HOMO→LUMO+2 (5.7%)
	S_0-T_1	420	2.95	0.0000	HOMO-1→LUMO (89.2%)
	S_0-T_2	376	3.30	0.0000	HOMO-3→LUMO (64.8%) HOMO-3→LUMO+2 (20.8%)
	S_0-T_3	350	3.54	0.0000	HOMO-2→LUMO+1 (72.3%) HOMO-5→LUMO+1 (7.0%)
	S_0-T_4	349	3.55	0.0000	HOMO-4→LUMO (40.1%) HOMO→LUMO (25.5%)
	S_0-T_5	342	3.62	0.0000	HOMO→LUMO (35.3%) HOMO-4→LUMO (23.2%) HOMO-1→LUMO+2 (7.5%) HOMO→LUMO+5 (6.5%)

Table S3. Spin-orbit coupling matrix elements (SOCME) of **NBO-mSAF** and **NBO-pSAF** at M062X/def2svp level.

λ_{SOC}	**NBO-mSAF**	**NBO-pSAF**
T_1-S_1	0.034	0.025
T_2-S_1	0.380	0.381
T_3-S_1	0.002	0.001
T_4-S_1	0.289	0.131
T_5-S_1	0.293	0.242
T_1-S_2	0.299	0.215
T_2-S_2	0.133	0.017
T_3-S_2	0.008	0.002
T_4-S_2	0.095	0.172
T_5-S_2	0.676	0.148

Table S4. Photovoltaic performance parameters in various solvents (n-hexane, toluene, tetrahydrofuran, dichloromethane, N, N-dimethylformamide, acetonitrile).

Emitter	**NBO-mSAF**		**NBO-pSAF**	
Solvent	λ_{em} (nm)	FWHM (nm)	λ_{em} (nm)	FWHM (nm)
Hex	448	28	438	18
Tol	458	28	446	20
THF	460	30	446	26
DCM	464	31	450	28
DMF	468/552	--	458/562	--
ACN	468/556	--	458/562	--

Table S5. Detailed photophysical data used to calculate the excited state dipole moments (μ_e) of **NBO-mSAF** and **NBO-pSAF**.

Emitter		**NBO-mSAF**			**NBO-pSAF**		
Solvent	f	λ_a (nm)	λ_f (nm)	ν_a-ν_f (cm^{-1})	λ_a (nm)	λ_f (nm)	ν_a-ν_f (cm^{-1})
Hexane	0.001	438	448	510	429	438	479
Toluene	0.014	440	458	893	432	446	727
Isopropyl ether	0.145	438	452	707	428	440	637
Chloroform	0.148	439	458	945	430	448	934
Ethyl ether	0.167	438	454	805	428	442	740
Ethyl acetate	0.200	438	458	997	429	446	888
THF	0.210	439	460	1040	430	446	834
DCM	0.217	439	464	1227	430	450	1033
DMSO	0.264	442	470/553	1348/4541	431	454/572	1175/5719
DMF	0.276	440	468/552	1360/4611	431	458/562	1368/5408
Acetone	0.284	438	462	1186	428	448/543	1043/5002
Acetonitrile	0.305	436	468/556	1568/4950	428	458/562	1530/5570
MeOH	0.309	438	458	997	427	446/550	998/5237

Table S6. Published photophysical data of the **NBO** emitters.

Emitter	Φ_{PL} [%]	Φ_{PF} [%]	Φ_{DF} [%]	τ_{PF} [ns]	τ_{DF} [μs]	K_r [10^7 s^{-1}]	K_{nr} [10^6 s^{-1}]	K_{ISC} [10^7 s^{-1}]	K_{RISC} [10^4 s^{-1}]
NBO[11]	99.0	--	--	7.7	86.6	11.1	--	1.4	1.2

Table S7. Summary of the sensitizer-free devices performance of **NBO-mSAF** and **NBO-pSAF** in 26DCzPPy host.

Emitter	Doping Ratio	V_{on} [V]	λ_{EL} [nm]	FWHM [nm]	L_{max} [cd m^{-2}]	CE_{max} [cd A^{-1}]	PE_{max} [lm W^{-1}]	$EQE_{max/1000}$ [%]	CIE (x,y)
NBO-mSAF	3 wt%	4.4	464	27	6892	21.6	15.4	25.9/6.4	(0.133,0.094)
	6 wt%	4.4	466	28	8201	27.7	19.3	29.5/6.0	(0.128,0.114)
	10 wt%	4.4	467	29	7282	24.4	17.4	24.9/4.7	(0.129,0.121)
NBO-pSAF	3 wt%	4.6	449	25	3355	8.2	5.6	17.2/4.9	(0.149,0.043)
	6 wt%	4.5	451	26	4639	11.0	7.7	20.5/5.7	(0.147,0.048)
	10 wt%	4.6	451	25	4347	10.7	7.3	19.5/4.4	(0.147,0.050)

Table S8. Summary of the sensitizer-free devices performance of **NBO-mSAF** and **NBO-pSAF** in PPF host.

Emitter	Doping Ratio	V_{on} [V]	λ_{EL} [nm]	FWHM [nm]	L_{max} [cd m^{-2}]	CE_{max} [cd A^{-1}]	PE_{max} [lm W^{-1}]	$EQE_{max/1000}$ [%]	CIE [x,y]
NBO-mSAF	3 wt%	4.2	468	34	1157	12.5	9.4	11.5/1.1	(0.126,0.147)
	6 wt%	3.4	472	34	2857	21.9	20.2	17.7/1.7	(0.120,0.180)
	10 wt%	3.6	472	34	2276	16.1	14.0	13.2/1.5	(0.125,0.174)
NBO-pSAF	3 wt%	4.6	454	32	593	9.8	6.7	14.2/2.1	(0.144,0.069)
	6 wt%	3.8	456	32	1029	13.0	10.7	16.1/1.2	(0.142,0.087)
	10 wt%	4.0	456	32	1188	12.6	9.9	13.4/1.1	(0.145,0.105)

6. References

1 I. S. Park, M. Yang, H. Shibata, N. Amanokura and T. Yasuda, *Adv. Mater.*, 2022, **34**, 2107951.

2 I. S. Park, H. Min and T. Yasuda, *Angew. Chem. Int. Ed.*, 2022, **61**, e202205684.

3 J. Park, J. Lim, J. H. Lee, B. Jang, J. H. Han, S. S. Yoon and J. Y. Lee, *ACS Appl. Mater. Interfaces*, 2021, **13**, 45798–45805.

4 C.-Y. Chan, S. Madayanad Suresh, Y.-T. Lee, Y. Tsuchiya, T. Matulaitis, D. Hall, A. M. Z. Slawin, S. Warriner, D. Beljonne, Y. Olivier, C. Adachi and E. Zysman-Colman, *Chem. Commun.*, 2022, **58**, 9377–9380.

5 J. Jin, M. Chen, H. Jiang, B. Zhang, Z. Xie and W.-Y. Wong, *ACS Mater. Lett.*, 2024, 3246–3253.

6 X. Huang, Y. Xu, J. Miao, Y.-Y. Jing, S. Wang, Z. Ye, Z. Huang, X. Cao and C. Yang, *J. Mater. Chem. C*, 2023, **11**, 11885–11894.

7 Y. Xu, J. Han, N. Li, Z. Huang, J. Miao and C. Yang, *J. Mater. Chem. C*, 2023, **11**, 13733–13739.

8 H. Tanaka, S. Oda, G. Ricci, H. Gotoh, K. Tabata, R. Kawasumi, D. Beljonne, Y. Olivier and T. Hatakeyama, *Angew. Chem. Int. Ed.*, 2021, **60**, 17910–17914.

9 X. Luo, H. Ni, A. Lv, X. Yao, H. Ma and Y. Zheng, *Adv. Opt. Mater.*, 2022, **10**, 2200504.

10 J. Liu, L. Chen, X. Wang, Q. Yang, L. Zhao, C. Tong, S. Wang, S. Shao and L. Wang, *Macromol. Rapid Commun.*, 2022, **43**, 2200079.

11 G. Liu, H. Sasabe, K. Kumada, H. Arai and J. Kido, *Chem. – Eur. J.*, 2022, **28**, e202201605.

12 J. Han, Z. Huang, X. Lv, J. Miao, Y. Qiu, X. Cao and C. Yang, *Adv. Opt. Mater.*, 2022, **10**, 2102092.

13 Z. Yan, L. Yuan, Y. Zhang, M. Mao, X. Liao, H. Ni, Z. Wang, Z. An, Y. Zheng and J. Zuo, *Adv. Mater.*, 2022, **34**, 2204253.

14 J. Jin, C. Duan, H. Jiang, P. Tao, H. Xu and W. Wong, *Angew. Chem. Int. Ed.*, 2023, **62**, e202218947.

15 K. R. Naveen, J. H. Oh, H. S. Lee and J. H. Kwon, *Angew. Chem. Int. Ed.*, 2023, **62**,

e202306768.

16 X. He, J. Lou, B. Li, X. Dong, F. Zhong, W. Liu, X. Feng, D. Yang, D. Ma, Z. Zhao, Z. Wang and B. Z. Tang, *Adv. Mater.*, 2024, **36**, 2310417.

17 J. Hu, Y. Wei, X. Wang, X. Liang, X. Liao, L. Yuan, H. Ni and Y. Zheng, *Adv. Opt. Mater.*, 2024, 2302987.

18 Y. Yin, X. Lai, Q. Ma, H. Ma, W. Zhu, J. Y. Lee and Y. Wang, *Adv. Mater.*, 2024, **36**, 2313656.

19 T. Lu and F. Chen, *J. Comput. Chem.*, 2012, **33**, 580–592.